Journal of Power Sources 196 (2011) 10762–10774

Contents lists available at SciVerse ScienceDirect

Journal of Power Sources

journal homepage: www.elsevier.com/locate/jpowsour

Effect of electrodeposition conditions on the electrochemical capacitive behavior of synthesized manganese oxide electrodes

Banafsheh Babakhani, Douglas G. Ivey*

Department of Chemical and Materials Engineering, University of Alberta, Edmonton, Alberta, Canada T6G 2V4

ARTICLE INFO

Article history:
Received 26 July 2011
Received in revised form 24 August 2011
Accepted 24 August 2011
Available online 1 September 2011

Keywords:
Electrodeposition
Electrochemical capacitor
Manganese oxide
Characterization
Voltammetry

ABSTRACT

Galvanostatic electrodeposition techniques were applied for the preparation of novel electroactive manganese oxide electrodes. The effects of supersaturation ratio on the morphology and crystal structure of electrodeposited manganese oxide were studied. Manganese oxide electrodes were synthesized by anodic deposition from acetate-containing aqueous solutions on Au coated Si substrates through the control of nucleation and growth processes. By changing deposition parameters, a series of nanocrystalline manganese oxide electrodes with various morphologies (continuous coatings, rod-like structures, aggregated rods and thin sheets) and an antifluorite-type crystal structure was obtained. Detailed chemical and microstructural characterization of as-deposited electrodes was conducted using SEM, TEM and AAS. Manganese oxide thin sheets show instantaneous nucleation and single crystalline growth, rods have a mix of instantaneous/progressive nucleation and polycrystalline growth and continuous coatings form by progressive nucleation and polycrystalline growth.

In addition, the electrochemical behavior was investigated by cyclic voltammetry. The experimental results show that manganese oxide electrodes, with rod-like and thin sheet morphology, exhibited enhanced electrochemical performance. The highest specific capacitance (~230 F g^{-1}) and capacitance retention rates (~88%) were obtained for manganese oxide thin sheets after 250 cycles in 0.5 M Na_2SO_4 at 20 mV s^{-1}.

1. Introduction

Electrochemical capacitors are currently receiving considerable attention, since they are extremely useful as energy storage devices in systems requiring quick bursts of energy such as portable electronic devices [1].

It is believed that surface morphology, which depends on the preparation method and processing parameters, significantly affects the capacitive behavior of electrode materials. Therefore, the fabrication of materials with appropriate morphology has become an important strategy to enhance the electrochemical performance of electrode materials. One-dimensional (1D) nanomaterials such as nanowires [2], nanorods [3], nanotubes [4] and two-dimensional (2D) nanosheets [5] are reported to exhibit outstanding charge storage properties, because they have large surface areas for charge storage and fast redox reactions. Diffusion resistance in the solid phase can be mitigated by shortening the diffusion paths [2,6–11].

Transition metal oxides are suitable materials to host small ions like H^+ and alkaline cations (Li^+, Na^+, K^+) during intercalation/deintercalation processes, which make them suitable materials for energy storage devices [12]. Among different transition metal oxides, manganese oxide has attracted considerable attention due to its high energy density, low cost, natural abundance and environmentally friendly nature. In recent years, electrodeposition techniques [13–18] have been increasingly explored due to their relatively easy and accurate control of the surface microstructure of deposited films by changing deposition variables, such as the electrolyte, deposition potential and bath temperature, to produce novel electroactive materials [19,20]. Many investigations have attributed the capacity of manganese dioxides to their structural, morphological and compositional characteristics [21–25]. Generally, most important physicochemical properties of manganese dioxide deposits depend on electrokinetic phenomena during the synthesis process. In general, it is postulated that oxidation of Mn^{2+} to MnO_2 occurs [26–28].

$$Mn^{2+} + 4OH^- \rightarrow MnO_2 + 2H_2O + 2e^- \quad (1)$$

By adjusting the deposition parameters, it is possible to modify the electrocrystallization process of MnO_2. This process can

* Corresponding author. Tel.: +1 780 492 2957; fax: +1 780 492 2881.
E-mail address: doug.ivey@ualberta.ca (D.G. Ivey).

0378-7753/$ – see front matter © 2011 Elsevier B.V. All rights reserved.
doi:10.1016/j.jpowsour.2011.08.102

be controlled via two fundamental electrokinetic phenomena, i.e., nucleation and growth of crystal grains. Generally, nucleation is either instantaneous or progressive and subsequent growth of nuclei is either two dimensional (2D) or three-dimensional (3D). It is believed that the nucleation mechanism during electrodeposition depends strongly on the bath composition, pH value of the electrolytes, overpotential (current density) and solution temperature [29,30].

Morphology-controlled growth can generally be achieved by controlling the deposition parameters. Manganese oxide electrodes with different surface morphologies, such as equiaxed and agglomerated particles [23], fibrous features (micro- and nano-scale fibers) [24], rod-like morphologies and aggregated rods [21,25], can be obtained under different electrodeposition conditions. The authors have been able to prepare manganese oxide with a rod-like morphology, without a template, through anodic deposition from a 0.01 M manganese acetate solution at various deposition current densities. Deposits prepared at a current density of 5 mA cm^{-2} showed the best capacitance (185 F g^{-1}) and retention (~75% of the original value – ~139 F g^{-1}) after 250 cycles in 0.5 M Na_2SO_4 at a scan rate of 20 mV s^{-1} [21]. However, there still has been little done to clarify the formation mechanism of manganese oxide electrodes and the relationship between the synthesis parameters and morphological, structural and electrochemical properties of electrodes. One of the authors [31] has shown that the morphology of manganese oxides is qualitatively determined by the supersaturation ratio (S), which affects the reaction kinetics in aqueous solutions. As the supersaturation ratio is increased, the deposition rate increases leading to the formation of several different morphologies from interconnected nanosheets (low S values) to columnar structures to discrete oxide clusters to petal- and flower-like morphologies to continuous coatings (high S values) with equiaxed and fibrous features [31]. However, the nucleation and growth mechanisms for manganese oxide electrodes with different morphologies are still not clarified.

This paper reports on the synthesis and nucleation and growth mechanisms of manganese oxide electrodes prepared from manganese acetate-containing aqueous solutions under various deposition parameters, i.e., current density, electrolyte composition and pH, deposition temperature and time, and presents a detailed electrochemical, morphological and structural analysis of electrochemically synthesized manganese oxide electrodes. The relationship between the physicochemical features of manganese oxide electrodes and the corresponding electrochemical behavior of the electrodes is investigated.

Manganese acetate-containing solutions are used, rather than other manganese components or additives, in this paper since high surface area morphologies such as rod-like structures are attainable from this electrolyte without any additives or the use of templates [21]. In addition, Rangappa et al. [32] have used anodic processes to produce Mn(4+) acetate and Mn(4+) sulfate. They observed that Mn(3+) acetate was significantly more stable than Mn(3+) sulfate, which indicates a thermodynamic favorability in the kinetics of oxidizing the acetate vs. the sulfate. A stable intermediate Mn(3+) species increases the reaction rate producing Mn(4+) as the final product. Therefore, manganese acetate allows for more rapid deposition at fixed potentials relative to manganese sulfate [32]. Moreover, it is suggested that in order to grow 1D nanostructures through template-free electrodeposition, the targeted materials must have intrinsic crystal structures that will form along one of the crystal axis or alternatively some growth modifier must be employed [33]. However, template-free electrodeposition has only been used for a limited set of materials. It is highly desirable to widen the applicability of this approach to a broader set of materials. Fully understanding the growth mechanism during the electrodeposition process and finding out the crucial parameters to control anisotropic growth are required to extend the applicability range of template-free electrodeposition of 1D nanostructures.

2. Experimental

Manganese oxide coatings were deposited from acetate-containing aqueous solutions ($Mn(CH_3COO)_2$) with various concentrations, i.e., from 0.003 to 0.05 M onto Au (500 nm thick) coated Si substrates (15 mm × 8 mm × 1 mm). Coatings were fabricated through anodic electrodeposition using galvanostatic control, with current densities ranging from 0.25 to 35 mA cm^{-2}. A platinum mesh with the same dimensions as the working electrode and a saturated calomel electrode (SCE) were used as the counter and reference electrodes, respectively. The counter electrode was placed vertically 20 mm away from the vertical working electrode. The deposition temperatures were controlled with a hot water bath and deposits were synthesized at 25, 60 and 85 °C. Electrolyte pH values were adjusted using dilute H_2SO_4 and NaOH solutions and deposits were synthesized at pH values of 5–8.5. Deposition times varied from 3 to 10 min. After electrodeposition, the working electrodes were rinsed with deionized water, dried at room temperature in air and then stored in a vacuum desiccator.

The morphology of as-deposited and cycled manganese oxide deposits were investigated using a Hitachi S-2700 scanning electron microscope (SEM) operated at 20 kV and equipped with an ultra-thin window (UTW) X-ray detector. The crystal structure and grain size/distribution of manganese oxide deposits were investigated using a JEOL 2010 transmission electron microscope (TEM) operated at 200 kV and equipped with an UTW X-ray detector. For TEM analysis, an electron transparent sample was prepared by scraping some of a deposit from the substrate and then ultrasonically dispersing the residue in ethanol or methanol for 10 min. One or two drops of the suspension were deposited onto a C-coated, Cu grid (300 mesh). After evaporation of the ethanol or methanol, samples were ready for TEM analysis.

In order to determine the electrochemical behavior of the manganese oxide electrodes, a Gamry PC4/750 potentiostat/galvanostat was used for cyclic voltammetry (CV) in an electrolyte containing 0.5 M Na_2SO_4 at room temperature. A three-electrode cell configuration was applied and consisted of a manganese oxide deposit on Au coated Si as the working electrode, a platinum (Pt) mesh as the counter electrode and a saturated calomel electrode (SCE) as the reference electrode. Cyclic voltammograms were recorded between −0.1 and 0.9 V vs. SCE at a scanning rate of 20 mV s^{-1}. To determine the specific capacitance C (F g^{-1}) of the active material, voltammetric charge Q (C) was obtained by integrating either the oxidative or the reductive parts of the cyclic voltammogram. This charge was subsequently divided by the mass of active material m (g) in the electrode and the width of the potential window of the cyclic voltammogram ΔE (V), i.e., $C = Q/(\Delta E m)$. The mass of the deposits was determined from the weight difference between the Au coated Si electrode before and after anodic deposition, as measured using a microbalance (Sartorius BP211D) with an accuracy of 10 μg.

The manganese content in 0.5 M Na_2SO_4 electrolytes after 2 and 250 cycles for various manganese oxide deposits was determined using a VARIAN 220 FS atomic absorption spectrometer (AAS).

Electrochemical impedance spectroscopy (EIS) measurements were conducted on cycled manganese oxide electrodes after 250 cycles in constant voltage mode (0.2 V vs. SCE) by sweeping frequencies from 100 kHz to 10 mHz at an amplitude of 5 mV.

3. Results and discussion

3.1. Surface morphology and structure of manganese oxide deposits

3.1.1. Effect of deposition current density

Nucleation strongly depends on the overpotential (current density) during electrochemical deposition. According to Faraday's law, the quantity of an electrochemical reaction at an electrode is proportional to the amount of electric charge. Therefore, for all deposition current densities, deposition rate can be estimated from [34]

$$V = \frac{i_k \eta_k E}{\rho} \quad (2)$$

where V is deposition rate, i_k is current density, η_k is current efficiency, E is the electrochemical equivalent for Mn (0.29282 g $(Ah)^{-1}$) and ρ is the density of Mn (7.21 g cm^{-3}). According to Eq. (2), the deposition rate is correlated with the current density and current efficiency. At a constant current efficiency the relationship between the deposition rate and current density should be linear.

Manganese oxide electrodes were prepared from a 0.01 M manganese acetate solution (60 °C with natural pH (7.5)); depositions were done for 10 min. At low deposition current densities (0.25–1 mA cm^{-2}), nucleation rates are low, leading to the formation of only a few oxide nuclei on the electrode surfaces during the initial stages of electrodeposition. As such, a continuous layer is not formed initially on the surface under these conditions. Oxide particles serve as seeds for the growth of thin, single crystal sheets. Thin sheets have very smooth surfaces and grow preferentially on the seed layer. Therefore, a thin sheet morphology (Fig. 1a and b) is obtained. A transition from a thin sheet to a rod-like structure is observed at 2 mA cm^{-2} (Fig. 1c). At higher magnifications (inset of Fig. 1c) thin sheets are apparent within the growing rods. As the deposition current density is increased, both nucleation and growth rates increase and rod-like structures are formed at intermediate current densities (5–15 mA cm^{-2}) (Fig. 1d and e). The rods (~1–3 μm in diameter) [25] are oriented perpendicular to the surface of the substrate for deposits prepared at 5 mA cm^{-2}. Manganese oxides with both rod-like and thin sheet structures provide large surface areas.

A further increase in overpotential results in a greater increase in the nucleation and growth rate. Therefore, the diameter of the oxide rods increases slightly, while the spaces between oxide rods decrease dramatically. As a result, rods with slightly larger radii (~1.5–3.5 μm in diameter) are formed at higher current densities of 15 mA cm^{-2} (Fig. 1e). At even higher current densities (e.g., 20 mA cm^{-2}), aggregated rods are formed and these have larger diameters (~2–4 μm) [25] (Fig. 1f). It was reported previously that manganese oxide synthesized at lower deposition current densities (5 mA cm^{-2}) had more uniform, vertical and free-standing rods relative to deposits prepared at higher deposition current densities (>15 mA cm^{-2}) [21].

An additional increase in deposition current density (~35 mA cm^{-2}) leads to the formation of a more continuous, but still porous, coating (Fig. 1g). In summary, as the deposition current density is increased, the morphology of manganese oxide deposits changes from thin sheets to rod-like to aggregated rods to continuous coatings.

Manganese oxide thin sheets possess a higher crystallization degree relative to rods, aggregated rods and continuous coatings. Fig. 1h and i depicts a TEM bright field (BF) image and a corresponding selected area electron diffraction (SAED) pattern for several thin sheets. The SAED pattern is a single crystal pattern, which can be indexed to an antifluorite crystal structure with a zone axis close to a ⟨1 1 1⟩-type orientation, i.e., the sheet planes are parallel to {1 1 1}-type planes. This result indicates that the thin sheets are single crystalline manganese oxides.

3.1.2. Effect of concentration of manganese acetate in solution

Manganese oxide deposits were prepared from manganese acetate-containing solutions, with different concentrations, at 5 mA cm^{-2}, natural pH and 60 °C for 10 min. As the concentration of the Mn^{2+} species is varied from 0.003 to 0.05 M, various morphologies are observed. At higher manganese acetate concentrations (≥0.05 M), adhesion to the substrate was poor so morphological analysis could not be done. At a low solution concentration, the electrodeposition rate of MnO_2 ($Mn^{2+} + 4OH^- \rightarrow MnO_2 + 2H_2O + 2e^-$) is low. As shown in Fig. 2a and b, discrete oxide clusters are dominant for the lowest manganese acetate concentrations studied (0.003 and 0.005 M). The higher magnification SEM images (inset of Fig. 2a and b) show that the discrete oxide clusters are essentially numerous oxide thin sheets grown vertically on the substrate. At low manganese oxide concentrations, not enough manganese oxide nuclei are generated to form a continuous coating; therefore, discrete oxide clusters are formed. As the concentration is increased from 0.005 to 0.007 M, oriented morphologies (free-standing micron-scale manganese oxide rods with fibrous surfaces) are realized (Fig. 2c). When a solution with higher concentration (0.01 M manganese acetate) is used, free-standing manganese oxide rods similar to those obtained at the 0.007 M solution concentration are observed; however, the density of rods is higher (Fig. 2d). As the concentration is increased from 0.01 to 0.02 M, aggregated rods are formed (Fig. 2e) while continuous morphologies are produced for manganese oxide deposits prepared from a 0.03 M manganese acetate solution (Fig. 2f). Increasing the solution concentration has a similar effect on the morphology as an increase in current density, i.e., as the solution concentration increases the morphology changes from thin sheets to rod-like to continuous coatings.

TEM micrographs and an SAED pattern for manganese oxide nanocrystals prepared from a 0.005 M manganese acetate solution at 5 mA cm^{-2} (Fig. 2b) are shown in Fig. 2g and h. The BF image (Fig. 2g) reveals fibrous features for the manganese oxide. Also, thin sheets are grown interlaced with one another. It is apparent that, based on the dark field (DF) image (Fig. 2h) and SAED ring pattern (inset of Fig. 2h), the manganese oxide deposits consist of discrete oxide clusters with thin sheets within them, and possess a higher crystallization degree when compared with aggregated rods (Fig. 3e) and continuous coatings (Fig. 4h), as shown later. Manganese oxide, in this case, consists of crystalline grains less than 10 nm in size with an antifluorite-type structure, which is consistent with previous studies [21,25].

3.1.3. Effect of manganese acetate solution temperature

Fig. 3a–c depicts the morphologies of manganese oxide electrodes prepared from a 0.01 M manganese acetate solution at 5 mA cm^{-2} and natural pH, at room temperature and elevated temperatures. As shown in Fig. 3a, lower nucleation rates occur at room temperature, so that very few oxide nuclei form on the electrode surface during the initial stages of electrodeposition. As such, a continuous coating is not formed; instead discrete oxide particles are formed. There are numerous microcracks within the oxide coatings prepared at room temperature. As shown previously [21,25], manganese oxide deposits obtained at 60 °C have a well-ordered rod-like structure consisting of rods ~1–3 μm in diameter [21,25] (Fig. 3b), whereas the deposits obtained at the higher temperature of 85 °C (Fig. 3c) exhibit aggregated rods similar to that obtained at high current densities (20 mA cm^{-2} – Fig. 1f) and a high acetate concentration (0.02 M – Fig. 2b) during room temperature deposition. High temperatures result in a more fibrous morphology (inset

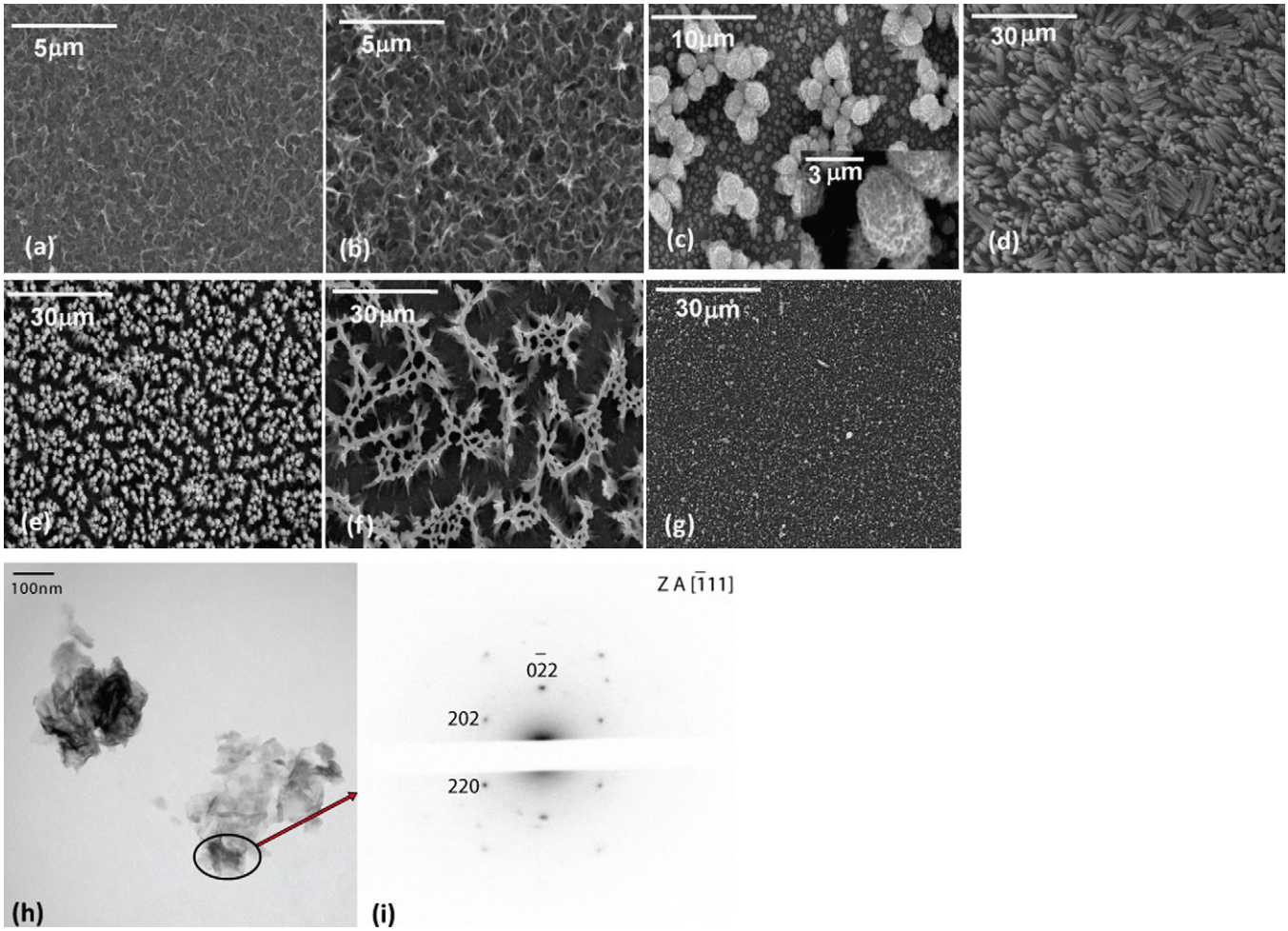

Fig. 1. SEM secondary electron (SE) plan view images of manganese oxide deposits prepared from 0.01 M $Mn(CH_3COO)_2$ solution at various current densities. (a) 0.25 mA cm^{-2}; (b) 1 mA cm^{-2}; (c) 2 mA cm^{-2}; (d) 5 mA cm^{-2}; (e) 15 mA cm^{-2}; (f) 20 mA cm^{-2}; (g) 35 mA cm^{-2}; (h and i) TEM BF image and SAED pattern of manganese oxide prepared at 1 mA cm^{-2} (natural pH = 7.5, and T = 60 °C for 10 min).

of Fig. 3c) while at low temperatures (room temperature) discrete oxide particles become predominant (inset of Fig. 3a).

Wang et al. [18] have shown that a higher temperature is preferable for the anisotropic growth of crystals and results in a product with higher aspect ratios [18]. Liang et al. [35] have reported that the surface morphology (surface area) is highly affected by electrolyte temperature [35]. As the temperature is increased, the morphology is changed from discrete oxide particles to rod-like to aggregated rods.

TEM micrographs and an SAED pattern for manganese oxide nanocrystals prepared at 85 °C (Fig. 3c) are shown in Fig. 3d and e. The TEM BF image (Fig. 3d) reveals some fibers with a thickness of several nanometers attached to the surface of the rods. The DF image shown in Fig. 3e reveals nanocrystalline grains with diameters less than 6 nm. Some larger grains from the Au seed layer are also visible in the DF image. The SAED pattern (inset of Fig. 3e) reveals that a nanocrystalline antifluorite-type structure is formed.

3.1.4. *Effect of manganese acetate solution pH*

According to the reaction for the electrodeposition of MnO_2 ($Mn^{2+} + 4OH^- \rightarrow MnO_2 + 2H_2O + 2e^-$), Mn^{2+} consumes OH^- anions to produce MnO_2. Therefore, higher pH values are more favorable for the formation of MnO_2, and the effect should be pronounced because of the prefactor of 4 in the above equation. Higher pH values lead to the formation of a large number of nuclei, and the surface coverage improves as pH is increased, so that a continuous coating is expected at high pH values. Fig. 4 shows SEM images of manganese oxide deposits prepared from a 0.01 M manganese acetate solution at 5 mA cm^{-2} and 60 °C for different electrolyte pH values.

The morphology changes with varying pH can be explained by considering the formation of intermediates of the Mn^{3+} species, such as MnOOH, during the electro-oxidation of Mn^{2+} to MnO_2. The physicochemical stability of MnOOH plays an important role in the morphology of MnO_2 deposits by inhibiting grain growth at the anode/electrolyte interface [36,37]. MnOOH is thermodynamically more stable at higher pH and dissolves in lower pH solutions. The nucleation rate is lower at low pH values (~5–6). As the solution pH increases from 5 to 8.5, various morphologies are observed. At a pH value of 5, oxide protrusions with fibrous features are formed on the surface (Fig. 4a). Thin sheets are apparent within the oxide protrusions at higher magnification (inset of Fig. 4a). The density of the oxide protrusions increases as the pH value is increased to 6. Rod-like structures are obtained as the pH value is increased to 7–7.5 (Fig. 4c and d), while continuous coatings are obtained when the manganese oxides are deposited in alkaline solutions, e.g., for solutions with pH = 8 and 8.5 as shown in Fig. 4e and f, respectively. The higher magnification SEM image (inset of Fig. 4f) shows that some of the oxide particles are connected together. To summarize, as pH is increased, the morphology is changed from oxide protrusions with fibrous features (thin sheets within the oxides), to rod-like to continuous coatings.

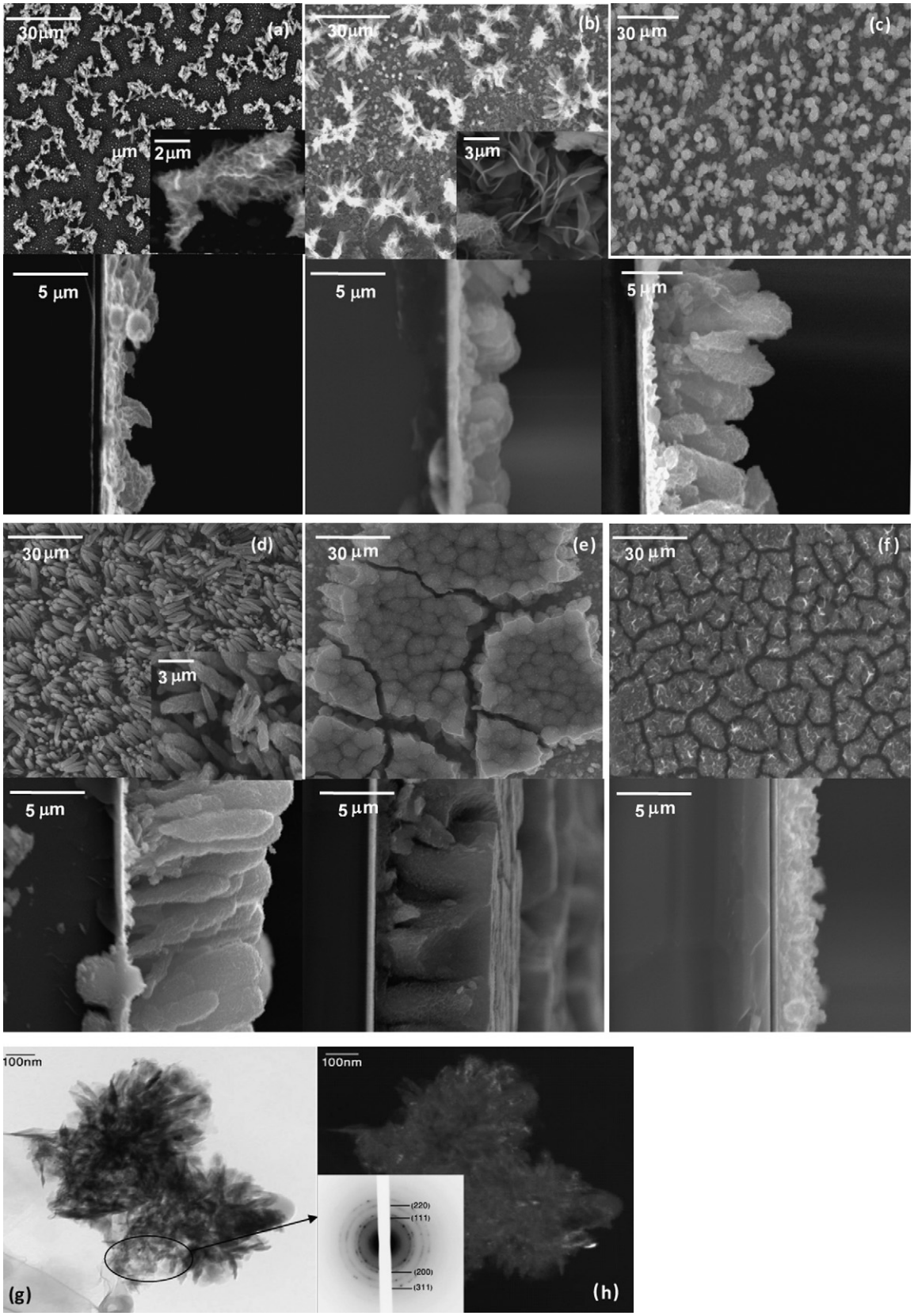

Fig. 2. SEM SE plan view and cross-sectional images of manganese oxide deposits prepared from (a) 0.003 M $Mn(CH_3COO)_2$ solution at 0.25 mA cm^{-2}; (b) 0.005 M; (c) 0.007 M; (d) 0.01 M; (e) 0.02 M; (f) 0.03 M $Mn(CH_3COO)_2$ solution at 5 mA cm^{-2} for 10 min (T = 60 °C and pH = 7.5); (g) 0.005 M $Mn(CH_3COO)_2$ – TEM BF image; (h) TEM DF image and SAED pattern from the circled region in (g).

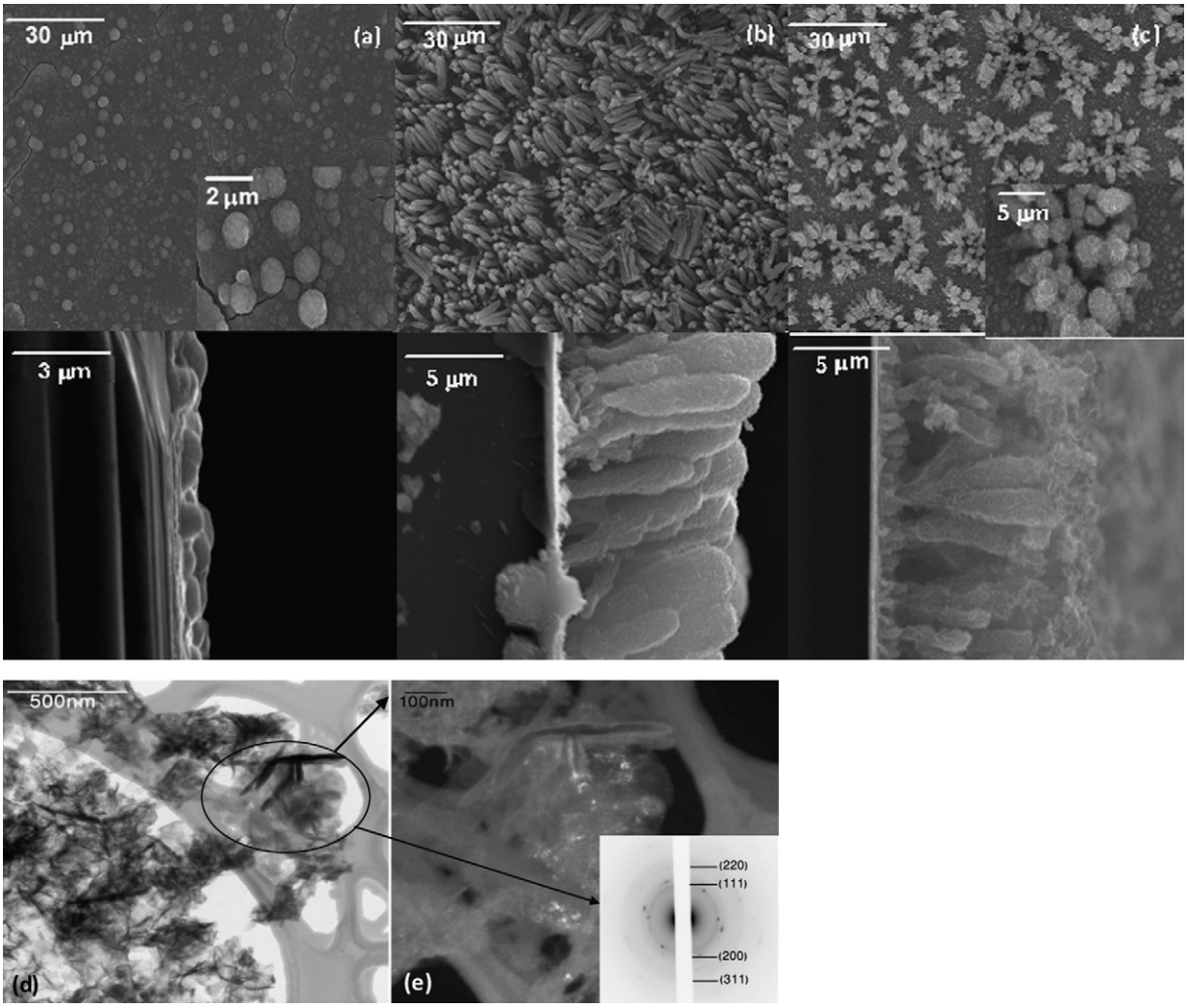

Fig. 3. SEM SE plan view and cross-sectional images of manganese oxide deposits prepared from a 0.01 M $Mn(CH_3COO)_2$ solution at 5 mA cm^{-2} for 10 min, and pH = 7.5. (a) T = 25 °C; (b) T = 60 °C; (c) T = 85 °C; (d) T = 85 °C - TEM BF image; (e) TEM DF image and SAED pattern from the circled region in (d).

Typical TEM BF and DF micrographs and a corresponding SAED pattern of an as-deposited, continuous manganese oxide coating (Fig. 4f) are shown in Fig. 4g and h. The BF image (Fig. 4g) also reveals fibrous surfaces for the manganese oxide particles. The DF image (Fig. 4h) shows that the manganese oxide consists of nanocrystalline grains with diameters less than 6 nm. The diffuse ring pattern (inset of Fig. 4h) confirms that the manganese oxide coating is nanocrystalline and the d-spacings can be indexed to the antifluorite-type structure. Comparing TEM analysis for manganese oxide deposits with different morphologies, it can be concluded that the deposition parameters do not affect the crystal structure of manganese oxide deposits but the crystallization degree is affected.

3.2. Effect of supersaturation ratio on formation of manganese oxide deposits

The schematic diagram in Fig. 5 correlates the changes in supersaturation ratio with morphological evolution for manganese oxide deposits during anodic electrodeposition.

Supersaturation ratio for a manganese acetate solution containing Mn^{2+} and OH^- ions for the formation of manganese oxide ($Mn^{2+} + 4\,OH^- = MnO_2 + 2\,H_2O + 2e^-$) can be defined as:

$$S = \frac{\alpha_{Mn^{2+}}\alpha_{OH^-}{}^4}{\alpha_{Mn^{2+},e}\alpha_{OH^-,e}{}^4} \quad (3)$$

where α_i and $\alpha_{i,e}$ are the actual and equilibrium activities, respectively, for component i. Under equilibrium conditions, $S = 1$. When $S > 1$, there is a driving force for nucleation and growth. Rastogi et al. [38] have shown that the frequency of nucleation increases with an increase in the supersaturation ratio and rapidly decreases as the supersaturation ratio is lowered below 10^3 [38]. Li et al. [39] have studied the influence of supersaturation ratio on the morphology of $BaSO_4$ crystals. Various morphologies from rod-like to snow-like (similar to aggregated rods in this work) to almost sphere-like (similar to the continuous coatings in this work) were produced by controlling supersaturation ratio. The supersaturation ratios were $\sim 2.3 \times 10^3$, 5.8×10^4 and 2.3×10^7 for rod-like, snow-like and sphere-like morphologies, respectively [39].

As the various deposition parameters, including current density, solution concentration, pH and temperature, are increased, the supersaturation ratio increases. The relationship between the activities of ions in solution and overpotential (current density) is given by the Nernst equation:

$$E = E_0 - \frac{RT}{ZF}\ln\frac{\alpha_{MnO_2}\alpha_{H_2O}{}^2}{\alpha_{Mn^{2+}}\alpha_{OH^-}{}^4} \quad (4)$$

$$\eta = E - E_0 \quad (5)$$

where η, Z, F, R, T, E_0 and E are the overpotential, the number of moles of electrons transferred in the cell reaction, Faraday's

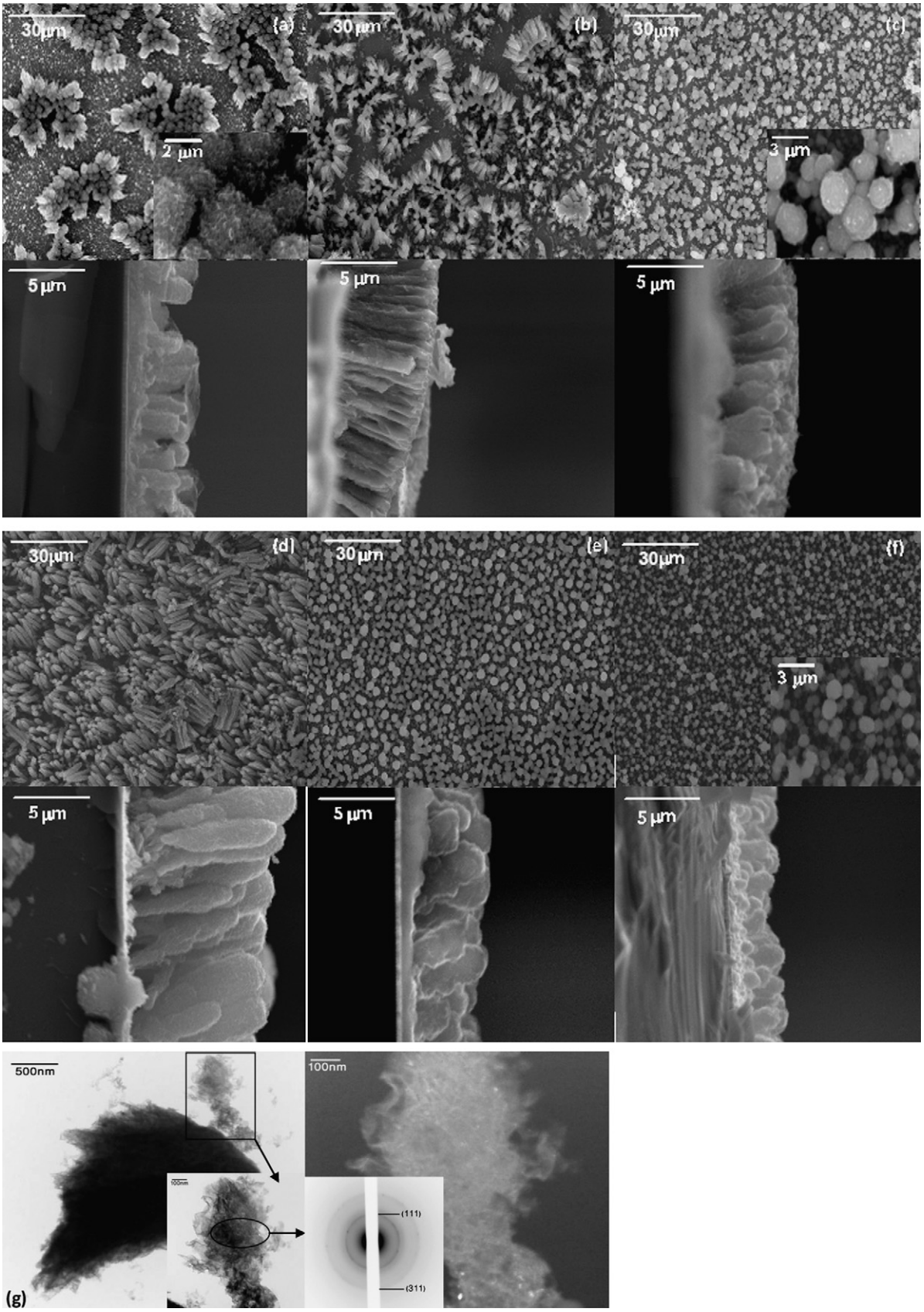

Fig. 4. SEM SE plan view and cross-sectional images of manganese oxide deposits prepared from a 0.01 M $Mn(CH_3COO)_2$ solution at 5 mA cm^{-2} for 10 min, and $T = 60\,^{\circ}C$. (a) pH = 5; (b) pH = 6; (c) pH = 7; (d) pH = 7.5; (e) pH = 8; (f) pH = 8.5; (g) pH = 8.5 – TEM BF image; (h) TEM DF image and SAED pattern from the circled region in (g).

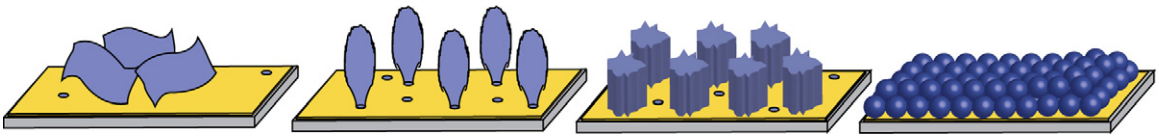

Fig. 5. Schematic diagram correlating manganese oxide morphology evolution with supersaturation ratio changes (thin sheets, rods, aggregated rods and non-uniform continuous coatings are formed as the current density, solution concentration, pH and temperature are increased).

constant, the gas constant, temperature, the standard cell potential (0.519 V vs. SCE at 298 K) and cell potential, respectively.

As the current density is increased, the cell potential increases which causes an increase in the overpotential value. Therefore, $(\alpha_{Mn^{2+}}\alpha_{OH^-}{}^4)$ is increased, while the equilibrium activities remain constant, leading to an increase in the supersaturation ratio.

Activities are directly proportional to the ion concentrations, so any increase in Mn^{2+} or OH^- concentration will cause an increase in S. For OH^- concentrations (or pH), the effect should be more pronounced because of the exponent of 4. OH^- activity increases with increasing pH according to:

$$\mathrm{pH} = 14 + \log\ \alpha_{OH^-} \tag{6}$$

In determining the effect of temperature on supersaturation ratio, it should be noted that the equilibrium activities are affected by changing the temperature. The reaction for formation of MnO_2 is endothermic ($\Delta H^\circ = 49.2\ \mathrm{kJ\ mol^{-1}}$ at 298 K). According to the van't Hoff equation

$$\frac{d\ \ln K}{d(1/T)} = -\frac{\Delta H^\circ}{R} \tag{7}$$

when the reaction is endothermic (ΔH° is positive), the equilibrium constant (K) increases with increasing temperature. This causes a reduction in $(\alpha_{Mn^{2+},e}\alpha_{OH^-,e}{}^4)$. Therefore, as the temperature is increased, the supersaturation ratio increases.

The relationship between the deposition rate and supersaturation ratio is shown in Eq. (8) [40].

$$V = kNS^n \tag{8}$$

where V is the deposition rate, k is the kinetic constant for a given temperature (Arrhenius-type dependence), N is proportional to the number of active sites on the surface, S is the supersaturation ratio and n is the effective order of the reaction [40]. Based on the above equation, as supersaturation ratio increases, the deposition rate is increased. The supersaturation ratio values, for deposits obtained at different current densities at 60 °C in this work, are calculated from Eqs. (2) and (3) as ~153 ($1\ \mathrm{mA\ cm^{-2}}$), 2.1×10^3 ($5\ \mathrm{mA\ cm^{-2}}$), 8.1×10^5 ($15\ \mathrm{mA\ cm^{-2}}$) and 1.3×10^7 ($30\ \mathrm{mA\ cm^{-2}}$) for thin sheets, rods, aggregated rods and continuous coatings, respectively. The average deposition rates ($V = \Delta m/\Delta t$), for the same temperature, are 2.5×10^{-4}, 3.3×10^{-4}, 3.6×10^{-4} and $4.2\times10^{-4}\ \mathrm{mg\ cm^{-2}\ s^{-1}}$ for thin sheets, rods, aggregated rods and continuous coatings, respectively. The S values are comparable to those reported by Li et al. [39] for similar structures. The natural logarithm of the deposition rate vs. natural logarithm of the supersaturation ratio for deposits prepared at 60 °C is plotted in Fig. 6. There is an approximately linear relationship but the value for n, determined from the slope of the line, is quite small (~0.04). According to Combes et al. [40], the value of n should be ≥1. Values of n equal to 1 and 2 are attributed to bulk diffusion controlled processes and spiral growth mechanisms, respectively. A value of n in excess of 2 corresponds to surface polynucleation. The small value for n is related to the assumption above that k and N are constant. The latter is a reasonable assumption, but k likely changes significantly as S is varied, since the current efficiency (η_k) varies markedly as the current density changes from 1 to $30\ \mathrm{mA\ cm^{-2}}$. In fact, η_k is ~90% at $1\ \mathrm{mA\ cm^{-2}}$ and only 50% at $30\ \mathrm{mA\ cm^{-2}}$.

3.3. Nucleation and growth mechanisms for manganese oxide deposits

There are two main nucleation mechanisms for electrodeposition, instantaneous and progressive. Instantaneous nucleation favors the growth of existing nuclei instead of the formation of new ones, achieving better crystalline quality relative to that for progressive nucleation [41]. Therefore, the single crystalline growth of thin sheets (Fig. 1h and i) at low supersaturation ratios and low deposition rates would be expected to follow an instantaneous nucleation mechanism with a constant number of nuclei. Fig. 7a shows the morphology of manganese oxide thin sheets prepared from a 0.01 M manganese acetate solution at $1\ \mathrm{mA\ cm^{-2}}$ (natural pH and $T = 60\ ^\circ\mathrm{C}$) for deposition times of 1–10 min. The plan view SEM images show that the number of nuclei are constant for different deposition times which confirms that manganese oxide thin sheets form by instantaneous nucleation.

Hwang et al. [42] have shown that progressive nucleation occurs on a larger number of active sites relative to instantaneous nucleation, resulting in the growth of compact grains. The nuclei not only form on substrate surface positions but also on previously formed nuclei [42].

The formation process for manganese oxide rods prepared from a 0.01 M manganese acetate solution at $5\ \mathrm{mA\ cm^{-2}}$ (natural pH and $T = 60\ ^\circ\mathrm{C}$) for different deposition times is shown in Fig. 7b. The number of nuclei on the surface for different deposition times is constant. Therefore, manganese oxide rods show instantaneous nucleation initially. However, TEM analysis shown in Fig. 3e for aggregated rods, and previous work for rods reported in [21] and [25], show that the rods are polycrystalline so that further formation is through progressive nucleation. Therefore, initial instantaneous nucleation is followed by progressive nucleation to form polycrystalline rods. For continuous manganese oxide deposits, the number of nuclei increases with deposition time from 1 to 10 min, which confirms the progressive nucleation mechanism for continuous coatings (Fig. 7c).

The formation mechanisms for manganese oxide deposits can also be rationalized by considering the effect of supersaturation ratio. Schematic diagrams for the different morphologies are shown in Fig. 8a–c. Thin sheets show instantaneous nucleation and single

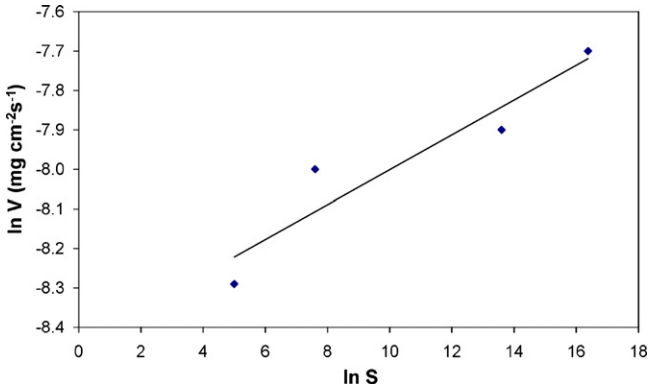

Fig. 6. Deposition rate vs. supersaturation ratio for deposits prepared at different current densities at 60 °C.

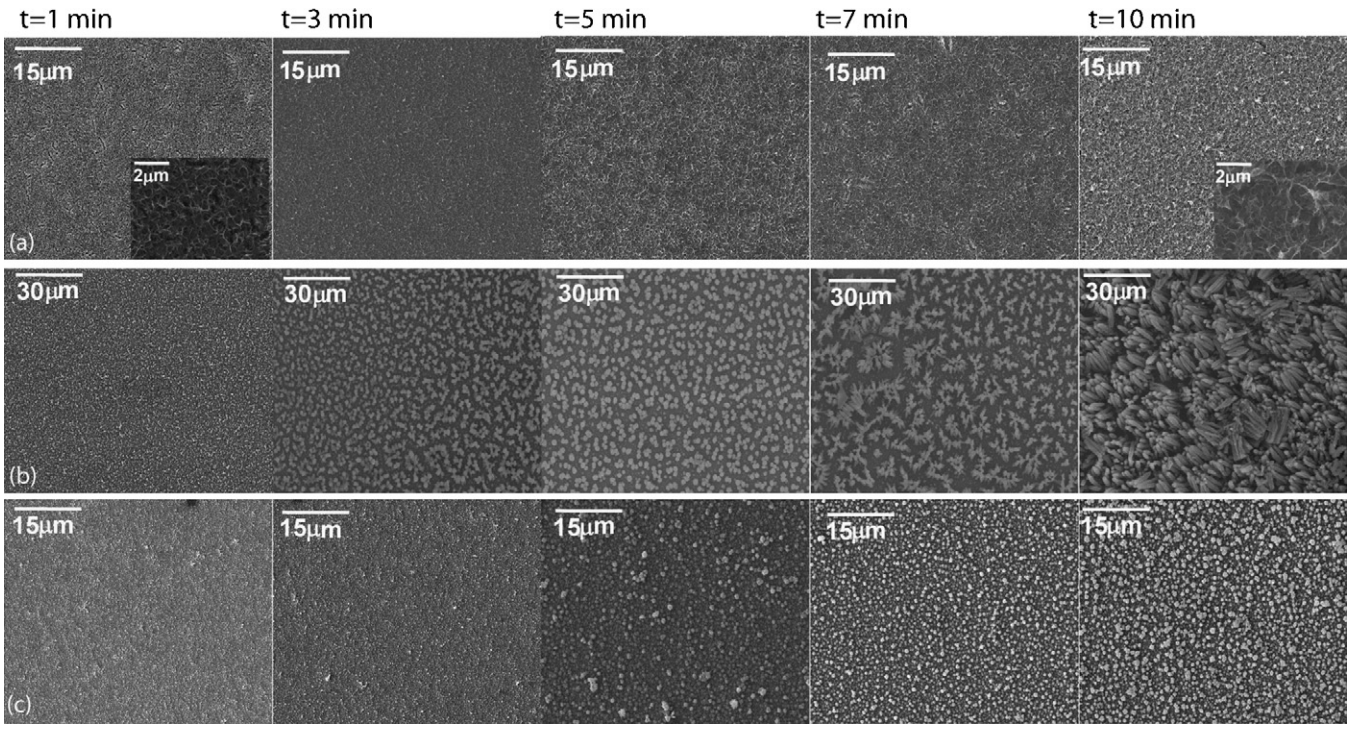

Fig. 7. SEM plan view images of manganese oxide deposits prepared from a 0.01 M $Mn(CH_3COO)_2$ solution at (a) 1 mA cm^{-2}; (b) 5 mA cm^{-2}; (c) 35 mA cm^{-2} – T = 60 °C, pH = 7.5 and depositions were done for 1, 3, 5, 7 and 10 min.

crystal growth (Fig. 8a) and are formed at very low supersaturation ratios. At low deposition current densities or solution concentrations, the very small supersaturation ratio provides only a few nucleation sites and the formation of only a few critical nuclei. Surface diffusion of ad-ions on the substrate allows for the growth of single crystal manganese oxide films. In fact, at very low supersaturation ratio, growth by surface diffusion is dominant [43]. This kind of growth mode leads to the formation of anisotropic crystals [44]. Thin sheets have high 2D anisotropy with thicknesses on the nanoscale and lateral dimensions on the microscale, as growth of the sheets is more favorable in the lateral direction compared with the thickness direction [45]. One reason for 2D growth is that low current densities and low reactant concentrations cause the reactions to proceed slowly. Thus, the initial nuclei have sufficient time to accommodate diffusion ad-ions and grow in the lateral directions, resulting in the formation of thin sheets [46]. Each thin sheet is a single crystal of manganese oxide with an antifluorite-type structure as shown in Fig. 1i. The lateral growth of manganese oxide does not occur on all faces but only on faces where the energy of incorporation of an ad-atom at the surface of the face is the lowest. Wang et al. [47] have shown that for FCC structures, the relative surface energies for crystallographic planes is: $\gamma(1\,1\,1) < \gamma(1\,0\,0) < \gamma(1\,1\,0)$ [47]. This is confirmed in Fig. 1i, where the thin sheets are shown to have a $\{1\,1\,1\}$-type orientation.

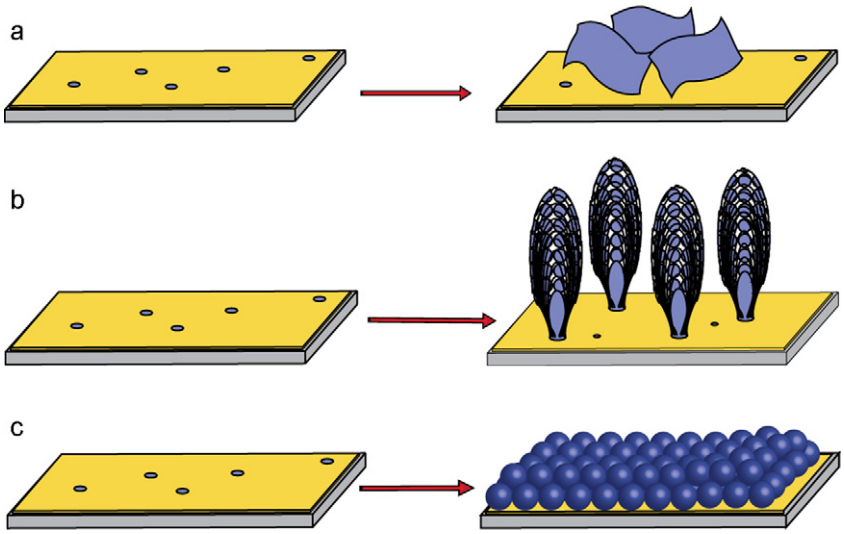

Fig. 8. Schematic diagrams showing nucleation and growth mechanisms for manganese oxide. (a) Thin sheet formation (instantaneous nucleation and single crystal growth); (b) rod formation (a mix of instantaneous/progressive nucleation and polycrystalline growth); (c) continuous coating formation (progressive nucleation and polycrystalline growth).

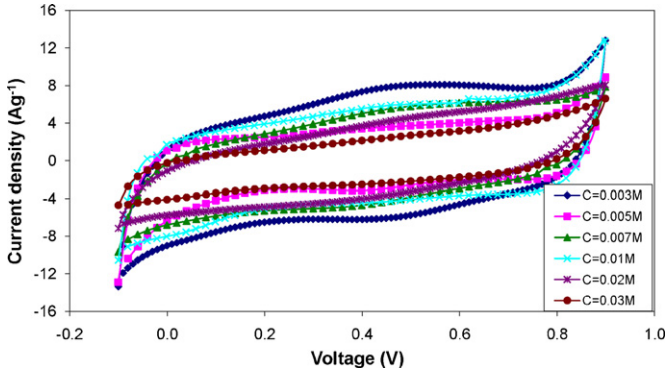

Fig. 9. Representative cyclic voltammogram taken from manganese oxide deposits prepared from a manganese acetate-containing solution at $i = 5\,mA\,cm^{-2}$, pH = 7.5, $T = 60\,^{\circ}C$ and $t = 10\,min$ (cycled in 0.5 M Na_2SO_4 for 2 cycles at $20\,mV\,s^{-1}$).

Nucleation for the rod-like structures is unlikely to be instantaneous alone, otherwise the rods would be expected to be single crystalline. Instead, a mix of instantaneous and progressive nucleation is proposed. Initial nuclei form instantaneously, but during rod formation additional nuclei, shown as small circles in Fig. 8b, form on the surface of growing rods. The number of nuclei on the surface is constant for different deposition times (Fig. 7b), which is characteristic of instantaneous nucleation. The growing rods are then preferential sites for the new nuclei as the electric field is higher locally, leading to progressive nucleation. This results in a preferential formation in the electric field direction, perpendicular to the substrate surface for polycrystalline manganese oxide rods. The atomic arrangement rate along the electric field direction is high, resulting in preferential growth perpendicular to the substrate and the formation of a rod-like structure since the growth rate of one direction is faster than that of the others [44].

As the supersaturation ratio is increased further, the nucleation rate is increased accordingly (Fig. 7c). The deposition rate increases, so that atoms do not have enough time to arrange on the lowest energy sites. As a result, the growth rate in all directions is almost the same, leading to a more continuous coating. Fig. 8c shows schematic diagrams for nucleation and growth of continuous coatings. Manganese oxide continuous coatings are polycrystalline in nature (Fig. 4h) and form through progressive nucleation.

3.4. Electrochemical properties of manganese oxide deposits

The capacitive behavior of electrode materials is generally characterized by means of cyclic voltammetry. Fig. 9 shows CV curves, after 2 cycles in 0.5 M Na_2SO_4, for manganese oxide deposits obtained for one of the deposition parameters discussed above (electrolyte concentration). The CV profiles of as-prepared manganese oxide deposits taken at a scan rate of $20\,mV\,s^{-1}$ show a nearly rectangular shape, indicating good pseudocapacitive behavior attributed to a continuous and reversible Faradaic redox transition of manganese oxide over the potential range. Comparison of the CV curves shown in Fig. 9 reveals that the enclosed areas for deposits with different morphologies are different, indicating a different charge-storage capability for the oxide films deposited.

Specific capacitance values, as a function of cycling, for manganese oxide deposits prepared under different deposition conditions are tabulated in Tables 1–4. The capacitance retention rates for manganese oxide with thin sheet and rod-like morphologies are higher than those observed for continuous manganese oxide deposits. It is apparent that manganese oxides, with a thin sheet morphology, exhibit the highest capacity and rate capability, followed by rod-like structures and then continuous coatings.

As described previously [21], electrode materials with ordered and high surface area structures have enhanced electrochemical characteristics. Large specific surface areas promote efficient contact between the active material and the electrolyte, providing more electrochemically accessible sites for electrochemical reactions relative to continuous coatings. In addition to supplying more accessible space for ions, electrodes with large surface area maintain sufficient electronic conductivity for solid-state electron transfer. Therefore, manganese oxide with thin sheet and rod-like structures can provide short diffusion path lengths to both ions and electrons giving rise to high charge–discharge rates. Manganese oxide thin sheets provide higher capacitance values and better capacitance retention rates relative to manganese oxide rods. Higher capacitance values may be attributed to lower thicknesses for the thin sheets compared to rods. Electrolyte ion transport is improved and solid-state diffusion distances for ions into the oxides are reduced, which enhance cation intercalation/deintercalation reactions compared to manganese oxide rods leading to higher specific capacitance values.

The loss in capacitance with electrochemical cycling can be attributed to several factors, such as increased manganese ion dissolution and morphological/structural changes [21]. TEM analysis of cycled manganese oxide thin sheets (not shown here) revealed that the crystal structure did not change, i.e., the antifluorite-type structure was maintained. The *d*-spacings were essentially the same ($\leq$2% difference on cycling), so that cycling did not appreciably affect the deposit crystal structure. However, as shown in [21], MnO_2 rods transformed to a more ordered hexagonal NiAs-type crystal structure after cycling. As such, fewer electrochemically active sites were available for fast ionic transport and charge transfer resulting. Therefore, structural changes can be considered as one of the factors for capacitance fading.

As described in [48], some Mn oxide dissolution as Mn^{2+} cations in the electrolyte is expected during cycling, based on the Mn-H_2O Pourbaix diagram. In addition, during forward cycling, some of the dissolved Mn^{2+} cations will be re-oxidized to MnO_2 and re-deposited on the electrode surface resulting in a morphology change for manganese oxide rods. This is another factor for capacitance reduction during cycling for manganese oxide rods. However, the morphology of manganese oxide thin sheets (not shown here) did not change much relative to the as-deposited sample.

It has been shown that the capacity fading is characteristic of progressive dissolution of electroactive material in the electrolyte during long term cycling [48,49]. Therefore, capacitance fading is mainly attributed to the loss of unstable manganese ions by dissolution in the electrolyte solution. The amount of dissolution, as determined through AAS measurements, was lower for manganese oxide thin sheets compared with rod-like structures. For manganese oxide rods, solution manganese levels of 0.17 and 0.25 ppm [25] were found after 2 and 250 cycles, respectively; for thin sheets, solution manganese levels were 0.15 and 0.17 ppm, respectively. Therefore, the manganese dissolution rate for rod-like structures is higher relative to thin sheets, which results in more capacitance reduction on cycling for rods relative to thin sheets.

Continuous coatings provide the lowest specific surface area relative to rods and thin sheets. Electron transfer through the denser continuous manganese oxide coatings is slower relative to rods and thin sheets. Also, ion diffusion transport of electrolytic species into the electrode material is more difficult for continuous coatings relative to rods and thin sheets due to lower specific surface areas. As

Table 1
Specific capacitance values for manganese oxide deposits prepared at different current densities (cycled in 0.5 M Na_2SO_4 at 20 mV s^{-1}).

Deposition current density (mA cm^{-2})	Specific capacitance after 2nd cycle (F g^{-1})	Specific capacitance after 250 cycles (F g^{-1})	Specific capacitance decrease after 250 cycles (%)	Deposit morphology
0.25	192	157	18	Thin sheets
1	230	202	12	Thin sheets
2	205	160	22	Thin sheets and rods
5	185	139	25	Rods
15	155	117	24	Rods
30	120	94	22	Aggregated rods
35	110	75	32	Continuous coatings

Table 2
Specific capacitance values for manganese oxide deposits prepared at different solution concentrations (cycled in 0.5 M Na_2SO_4 at 20 mV s^{-1}).

Solution concentration (M)	Specific capacitance after 2nd cycle (F g^{-1})	Specific capacitance after 250 cycles (F g^{-1})	Specific capacitance decrease after 250 cycles (%)	Deposit morphology
0.003	200	170	15	Thin sheets
0.005	164	135	18	Thin sheets and rods
0.007	180	140	22	Rods
0.01	185	139	25	Rods
0.02	155	112	28	Aggregated rods
0.03	145	85	41	Continuous coatings

Table 3
Specific capacitance values for manganese oxide deposits prepared at different solution pH values (cycled in 0.5 M Na_2SO_4 at 20 mV s^{-1}).

Solution pH	Specific capacitance after 2nd cycle (F g^{-1})	Specific capacitance after 250 cycles (F g^{-1})	Specific capacitance decrease after 250 cycles (%)	Deposit morphology
5	170	138	19	Oxide protrusions and thin sheets within them
6	175	143	18	Oxide protrusions and thin sheets within them
7	178	132	25	Rods
7.5	185	139	25	Rods
8	165	120	27	Continuous coatings
8.5	160	115	28	Continuous coatings

such, continuous coatings have the lowest capacitance values. The poor capacitance retention of continuous coatings is due to significantly higher manganese oxide dissolution rates relative to thin sheets and rods. For manganese oxide continuous coatings, solution manganese levels of 0.61 and 0.85 ppm were found after 2 and 250 cycles, respectively. The type of morphology can affect Mn dissolution during cycling. This is likely due to the trapping of soluble Mn ions within the electrode structure for rods and thin sheets, which enhances redeposition of Mn oxide on the electrode during forward cycling. Therefore, a large amount of active material is still available after cycling which results in improved electrochemical cyclability [50].

To further understand the capacitance behavior of manganese oxide electrodes prepared under different deposition conditions,

Table 4
Specific capacitance values for manganese oxide deposits prepared at different solution temperatures (cycled in 0.5 M Na_2SO_4 at 20 mV s^{-1}).

Solution temperature (°C)	Specific capacitance after 2nd cycle (F g^{-1})	Specific capacitance after 250 cycles (F g^{-1})	Specific capacitance decrease after 250 cycles (%)	Deposit morphology
25	123	75	39	Small oxide particles
60	185	139	25	Rods
85	147	115	22	Aggregated rods

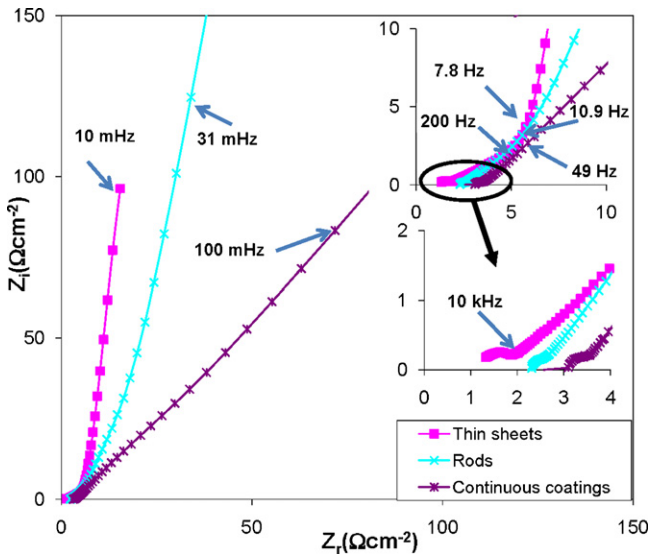

Fig. 10. Nyquist plots for manganese oxide deposits with different morphologies cycled at 20 mV s^{-1} (0.5 M Na_2SO_4 solution at 0.2 V vs. SCE) after 250 cycles.

EIS was applied to evaluate manganese oxide deposits after 250 cycles at 20 mV s^{-1}, by sweeping the frequency from 100 kHz to 10 mHz with a DC bias of 0.2 V. Manganese oxide deposits with thin sheet and rod-like structures were prepared from 0.01 M manganese acetate solution at 1 and 5 mA cm^{-2}, respectively and continuous coatings were prepared from 0.03 M manganese acetate solution at 5 mA cm^{-2} (natural pH, T = 60 °C for 10 min). The corresponding impedance spectra for manganese oxide electrodes with different morphologies are compared in Fig. 10. Each impedance spectrum can be divided into three regions corresponding to three processes. At very high frequencies (>10 kHz) small arcs are present, which account for the double layer (dl) processes. The small semicircles present at high frequencies (>50 Hz) are related to charge transfer processes [16]. Approximately straight lines with various slopes are present in the impedance plots within the low frequency range. These linear parts are typical of the capacitive response of porous electrode materials, which is related to the electrolyte diffusion process and cation intercalation–deintercalation processes [1]. Normally, a higher slope for the impedance line means a lower diffusive resistance for the electrolyte in the electrode. For better comparison, AC frequencies are shown on the Nyquist plots. At frequencies higher than ~10 kHz, the three plots show comparable electronic resistances (inset of Fig. 10). For frequencies ranging from ~200 Hz down to ~7.8 Hz, continuous coatings show a higher charge transfer resistance relative to thin sheets and rod-like deposits, as its plot shifts more along the real axis to higher resistances. The experimental impedance data was fit to an equivalent circuit using Zview, based on previous work [48]. The corresponding charge transfer resistances for the thin sheets and rods were ~0.5 and 0.58 Ω cm^2, respectively. However, the resistance value for continuous coatings was ~1.5 Ω cm^2. The higher charge transfer resistance for the continuous coating is attributed to slow electron transport through the electrode. Rod-like morphologies and thin sheets have lower charge transfer resistances due to short path lengths for electron transport. For frequencies from 7.8 Hz down to 0.1 Hz, thin sheets show the lowest diffusive resistance (1.65 Ω cm^2) followed by rod-like structures (1.80 Ω cm^2) and then continuous coatings (2.70 Ω cm^2). Porous electrodes may facilitate electrolyte transport and cation intercalation/deintercalation in thin sheets and rods relative to continuous coatings, which is supported by the reduced resistance values and improved capacitor responses. Also, the lower thickness dimension provides shorter diffusion paths for cation intercalation/deintercalation for thin sheets relative to rods.

4. Conclusions

Morphology-controlled growth of manganese oxide nanostructures prepared from acetate-containing aqueous solutions was investigated. A variety of nanostructured manganese oxide electrodes, all with an antifluorite-type crystal structure and including continuous coatings, rod-like structures, aggregated rods and thin sheets, were obtained by changing the supersaturation ratio which affects the nucleation and growth processes. The crystal structure of manganese oxide was not affected by the supersaturation ratio, but crystallization degree was affected. The investigation of nucleation and growth mechanisms for manganese oxide deposits with different morphologies revealed that thin sheets form by instantaneous nucleation and single crystal growth, continuous coatings show progressive nucleation and polycrystalline growth and rods have a mix of instantaneous/progressive nucleation and polycrystalline growth.

Electrochemical analysis of manganese oxide electrodes revealed that oriented structures such as manganese oxide rods and thin sheets exhibited superior capacitive behavior relative to continuous coatings. Also, thin sheets with lower thicknesses relative to rods had the highest specific capacitance (~230 F g^{-1}) and capacitance retention (~88% after 250 cycles) in 0.5 M Na_2SO_4 at 20 mV s^{-1}. Electrochemical impedance spectroscopy showed a lower double layer process resistance and charge transfer resistance for thin sheets and rod-like structures compared with continuous coatings. Also, Nyquist diagrams confirmed that manganese oxide thin sheets had the lowest diffusive resistance followed by rods and then continuous coatings.

Acknowledgements

The financial support from the Natural Sciences and Engineering Research Council (NSERC) of Canada and the metallized Si wafers provided by Micralyne Inc. are gratefully acknowledged. The authors would also like to thank R. Eslahpazir for assistance with the SEM and TEM analysis.

References

[1] B.E. Conway, Electrochemical Supercapacitors, Kluwer Academic/Plenum Press, New York, 1999.
[2] R. Liu, S.B. Lee, J. Am. Chem. Soc. 130 (2008) 2942.
[3] M.S. Wu, Y.H. Ou, Y.P. Lin, Electrochim. Acta 55 (2010) 3240.
[4] R. Xiao, S.I. Cho, R. Liu, J. Am. Chem. Soc. 129 (2007) 4483.
[5] H. Zheng, F. Tang, M. Lim, A. Mukherji, J. Power Sources 195 (2010) 680.
[6] D. Belanger, T. Brousse, J.W. Long, Electrochem. Soc. Interface 17 (1) (2008) 49.
[7] K. Naoi, P. Simon, Electrochem. Soc. Interface 17 (1) (2008) 34.
[8] C.C. Hu, K.H. Chang, M.C. Lin, Y.T. Wu, Nano Lett. 6 (2006) 2690.
[9] R.K. Sharma, A.C. Rastogi, S.B. Desu, Electrochim. Acta 53 (2008) 7690.
[10] W. Sugimoto, H. Iwata, Y. Yasunaga, Angew. Chem. Int. Ed. 42 (2003) 4092.
[11] Y.H. Lee, K.H. An, W.S. Kim, Y.S. Park, Adv. Mater. 13 (2001) 497.
[12] S.C. Pang, M.A. Anderson, J. Mater. Res. 15 (2000) 2096.
[13] M. Nakayama, T. Kanaya, R. Inoue, Electrochem. Commun. 9 (2007) 1154.
[14] S.E. Chun, S.I. Pyun, G.J. Lee, Electrochim. Acta 51 (2006) 6479.
[15] M. Toupin, T. Brousse, D. Belanger, Chem. Mater. 16 (2004) 3184.
[16] C.C. Hu, C.C. Wang, J. Electrochem. Soc. 150 (2003) A1079.
[17] M.S. Wu, P.J. Chiang, Electrochem. Commun. 8 (2006) 383.
[18] X. Wang, Y. Li, J. Chem. Eur. 9 (2003) 300.
[19] P.A. Nelson, J.M. Elliott, G.S. Attard, J.R. Owen, Chem. Mater. 14 (2002) 524.
[20] W.J. Zhou, D.D. Zhao, M.W. Xu, Electrochim. Acta 53 (2008) 7210.
[21] B. Babakhani, D.G. Ivey, J. Power Sources 195 (2010) 2110.
[22] H. Xia, J.K. Feng, H.L. Wang, M.O. Lai, L. Lu, J. Power Sources 195 (2010) 4410.
[23] W. Wei, X.W. Cui, W.X. Chen, D.G. Ivey, Electrochim. Acta 54 (2009) 2271.
[24] W. Wei, X. Cui, W. Chen, D.G. Ivey, J. Power Sources 186 (2009) 543.
[25] B. Babakhani, D.G. Ivey, Electrochim. Acta 55 (2010) 4014.
[26] A.S. Pilla, M.M. Duarte, C.E. Mayer, J. Electroanal. Chem. 569 (2004) 7.
[27] W.H. Kao, V.J. Weibel, J. Appl. Electrochem. 22 (1992) 21.
[28] S. Nijjer, J. Thonstad, G.M. Haarberg, Electrochim. Acta 46 (2000) 395.
[29] M. Gu, Electrochim. Acta 52 (2007) 4443.

[30] M.S. Wu, R.H. Lee, J. Electrochem. Soc. 156 (9) (2009) A737.
[31] W. Wei, X.W. Cui, W.X. Chen, D.G. Ivey, Electrochim. Acta 56 (2011) 1619.
[32] K.S. Rangappa, S. Chandraju, N.M. Madegowda, Int. J. Chem. Kinet. 30 (1998) 7.
[33] G. She, L. Mu, W. Shi, Recent Patent Nanotechnol. 3 (2009) 182.
[34] J.X. Kang, W.Z. Zhao, G.F. Zhang, Surf. Coat. Technol. 203 (2009) 1815.
[35] C.H. Liang, C.S. Hwang, J. Appl. Phys. 47 (6) (2008) 4682.
[36] Z. Rogulski, H. Siwek, I. Paleska, J. Electroanal. Chem. 543 (2003) 175.
[37] S. Nijjer, J. Thonstad, D.M. Haarberg, Electrochim. Acta 46 (2000) 395.
[38] A.C. Rastogi, K.S. Balakrishnan, J. Electrochem. Soc. 136 (1989) 1502.
[39] S. Li, J. Xu, G. Luo, J. Cryst. Growth 304 (2007) 219.
[40] C. Combes, M. Freche, C. Rey, J. Mater. Sci. 10 (1999) 231.
[41] H. Gomez, G. Riveros, D. Ramirez, J. Solid State Electrochem. (2011).
[42] B.J. Hwang, R. Santhanam, Y.L. Lin, J. Electrochem. Soc. 147 (2000) 2252.
[43] A.C. Rastogi, K.S. Balakrishnan, Sol. Energy Mater. Sol. Cells 36 (1995) 121.
[44] D. Chu, Y. Masuda, T. Ohji, Langmuir 26 (18) (2010) 14814.
[45] T. Shibata, K. Fukuda, Y. Ebina, T. Kogure, Adv. Mater. 20 (2008) 231.
[46] S. Yue, J. Lu, J. Zhang, Mater. Lett. 63 (2009) 2149.
[47] S.G. Wang, E.K. Tian, C.W. Lung, J. Phys. Chem. Solids 61 (2000) 1295.
[48] B. Babakhani, D.G. Ivey, Electrochim. Acta 56 (2011) 4753.
[49] Y.K. Zhou, M. Toupin, D. Belanger, F. Favier, J. Phys. Chem. Solids 67 (2006) 1351.
[50] K. Kinoshita, J.T. Lundquist, Electroanal. Chem. Interface Electrochem. 48 (1973) 157.